The effect of annealing on the elastoplastic response of isotactic polypropylene

Aleksey D. Drozdov*and Jesper deC. Christiansen
Department of Production
Aalborg University
Fibigerstraede 16, DK–9220 Aalborg, Denmark

Abstract

Four series of tensile loading–unloading tests are performed on isotactic polypropylene in the sub-yield domain of deformations at room temperature. In the first series, injection-molded specimens are used as produced, whereas in the other series the samples are annealed for 24 h at 120, 140 and 160 °C, which covers the low-temperature region and an initial part of the high-temperature region of annealing temperatures. A constitutive model is developed for the elastoplastic behavior of a semicrystalline polymer. The stress–strain relations are determined by five adjustable parameters that are found by fitting the experimental data. The effect of annealing is analyzed on the material constants.

Key-words: Isotactic polypropylene, Cyclic loading, Elastoplasticity, Yielding, Annealing

*Corresponding author, fax: +45 9815 3030, E–mail: drozdov@iprod.auc.dk

1 Introduction

This study deals with the elastoplastic behavior of injection-molded isotactic polypropylene (iPP) in isothermal uniaxial tests with small strains. Plastic deformations and yielding of iPP have been the focus of attention in the past decade, see, e.g., [1, 2, 3, 4, 5, 6, 7, 8, 9], to mention a few. This may be explained by numerous applications of polypropylene in industry (ranged from oriented films for packaging to nonwoven fabrics and reinforcing fibres).

Isotactic polypropylene is a semi-crystalline polymer containing three different crystallographic forms [10]: monoclinic α crystallites, hexagonal β structures, orthorhombic γ polymorphs, and "smectic" mesophase (arrays of chains with a better order in the longitudinal than in transverse chain direction). At rapid cooling of the melt (which is typical of the injection-molding process), α crystallites and smectic mesophase are mainly developed, whereas β and γ polymorphs are observed as minority components [11].

The characteristic size of α spherulites in injection-molded specimens is estimated as 100 to 200 μm [3, 11]. These spherulites consist of crystalline lamellae with thickness of 10 to 20 nm [3, 12]. A unique feature of α spherulites in iPP is the lamellar cross-hatching: development of transverse lamellae oriented in the direction perpendicular to the direction of radial lamellae in spherulites [10, 12].

The amorphous phase is located (i) between spherulites, (ii) in "liquid pockets" [13] between lamellar stacks inside spherulites, and (iii) between lamellae in lamellar stacks. It consists of (i) mobile chains between spherulites, in liquid pockets and between radial lamellae inside lamellar stacks, and (ii) chains with restricted mobility (the so-called "rigid amorphous fraction" [13]) in regions bounded by radial and tangential lamellae.

Stretching of iPP specimens induces inter-lamellar separation, rotation and twist of lamellae, fine and coarse slip of lamellar blocks and their fragmentation [1, 5], chain slip through the crystals, sliding and separation of tie chains [4, 7], and activation of the rigid amorphous fraction induced by disintegration of transverse lamellae. At large strains, these transformations result in cavitation, formation of fibrills and stress-induced crystallization [14].

Annealing and isothermal crystallization of iPP have attracted an essential attention in the past five years, see, e.g., [10, 12, 15, 16, 17, 18, 19]. Dramatic changes are observed in DSC (differential scanning calorimetry) traces of isotactic polypropylene driven by annealing at elevated temperatures (in the range from 110 to 170 °C). It is found that annealing in the low-temperature interval (between 110 and 150 °C) results in (i) a monotonical increase in the melting peak [10] and (ii) formation of a broad low-temperature shoulder (second endotherm) on a melting curve; the intensity of this shoulder grows with annealing temperature [18]. Annealing in the high-temperature interval (between 150 and 170 °C) causes transformation of the second endotherm into the main peak [18], which may be attributed to a second-order phase transition in the crystalline phase [19]. The critical temperature corresponding to this transition lies in the region between 157 [12] and 159 °C [19]. The morphological analysis reveals that transformations of the melting curves caused by annealing are accompanied by changes in the crystalline structure (a pronounced reduction in the level of cross-hatching with an increase in the annealing temperature).

Although the effect of annealing on the micro-structure of crystallites has been studied in detail, a little is known about the influence of thermal treatment on the mechanical behavior of iPP. Our studies on the viscoelastic response of isotactic polypropylene annealed in the low-temperature interval (between 110 and 130 °C) revealed that the relaxation process is strongly affected by annealing [20]. The aim of the present work is to evaluate the effect of thermal treatment on the elastoplastic response of iPP.

An important shortcoming of conventional elastoplasticity theories for solid polymers, see, e.g., [21, 22, 23, 24, 25], is that they are grounded on the concept of yield surface. According to that approach, below the yield strain $\epsilon_{\rm y}$ (which is associated with the point of maximum on a stress–strain curve), a specimen demonstrates the nonlinear elastic (or viscoelastic) response. This implies that the loading and unloading paths of stress–strain diagrams should coincide (provided that the strain rate is so large that the stress relaxation phenomenon may be disregarded). The experimental data presented in Section 2 show that this assumption is inapplicable to isotactic polypropylene, whose stress–strain curves for loading and unloading noticeably differ from each other even when the maximal strain in a cyclic test is far below the yield strain.

The objective of this paper is to develop constitutive equations for the elastoplastic behavior of a semicrystalline polymer that do not employ the concept of yield surface and to apply these relations in fit observations in tensile cyclic tests with maximal strains in the sub-yield interval of deformations.

To make a constitutive model tractable from the mathematical standpoint, we treat a semicrystalline polymer as an ensemble of meso-regions (MRs). A meso-domain is thought of as an equivalent network of macromolecules bridged by junctions. The mechanical behavior of a MR is associated with that of the amorphous phase, whereas the links between meso-domains that transmit the macro-strain to individual MRs reflect the responses of crystallites.

A meso-region is treated as a linear elastic medium, whereas deviations of the stress–strain curves in tensile tests from straight lines (that describe the response of a linear elastic solid) are attributed to sliding of junctions between chains with respect to their reference positions in a stress-free material. This is an essential simplification of the mechanism of micro-deformations, which is tantamount to the assumption that only the amorphous phase is altered under active loading, whereas the crystalline phase remains unchanged. Elastic deformation of spherulites, inter-lamellar separation and fine slip of lamellar blocks are not introduced into the model explicitly, but are taken into account implicitly in terms of "average" parameters that characterize sliding of junctions in meso-domains. This "generalized" sliding process is described by a plastic strain, $\epsilon_{\rm p1}$, whose rate of growth is assumed to be proportional to the rate of straining.

At unloading, junctions between chains in MRs move back to their initial positions with a decrease in the macro-strain ϵ. Because deformation of a semicrystalline polymer results in micro-fracture of crystallites, the plastic strain $\epsilon_{\rm p1}$ (that decreases together with the macro-strain ϵ) is not sufficient to describe morphological transformations under unloading. To account for coarse slip and disintegration of lamellar blocks at unloading, another plastic strain, $\epsilon_{\rm p2}$, is introduced, which increases in time with a rate proportional to the rate of work of external forces.

A similarity may be noted between splitting the plastic strain, $\epsilon_{\rm p}$, into two components,

ϵ_{p1} and ϵ_{p2}, where the latter quantity is altered at unloading only, and a phenomenological model for the Mullins effect in particle-reinforced elastomers [26]. According to the Ogden–Roxburgh concept, the difference between the stress–strain curves at active deformation and unloading is attributed to some damage parameter that changes along the unloading path of a deformation history only. An advantage of our model compared to the Ogden–Roxburgh approach is that the plastic strain, ϵ_{p2}, obeys a conventional flow rule in elastoplasticity, whereas the damage parameter introduced in [26] is governed by a kinetic equation whose physical meaning is not clear for semicrystalline polymers.

The exposition is organized as follows. Observations in uniaxial loading–unloading tensile tests are reported in Section 2. Kinetic equations for the plastic strains, ϵ_{p1} and ϵ_{p2}, are introduced in Section 3. Constitutive equations for a semicrystalline polymer at isothermal uniaxial loading are derived in Section 4. Adjustable parameters in the stress–strain relations are determined in Section 5 by matching the experimental data. A brief discussion of our findings is presented in Section 6. Some concluding remarks are formulated in Section 7.

2 Experimental procedure

Isotactic polypropylene (Novolen 1100L) was supplied by BASF (Targor). ASTM dumbbell specimens were injection molded with length 148 mm, width 10 mm and thickness 3.8 mm. Uniaxial tensile tests were performed at room temperature on a testing machine Instron–5568 equipped with electro-mechanical sensors for the control of longitudinal strains in the active zone of samples. The tensile force was measured by a standard load cell. The longitudinal stress, σ, was determined as the ratio of the axial force to the cross-sectional area of stress-free specimens.

Four series of experiments were performed. In the first series, the specimens were used as produced. In the other series, the samples were annealed prior to testing for 24 h at the temperatures 120, 140 and 160 °C and slowly cooled by air. To minimize the effect of physical aging, mechanical tests were carried out at least one day after thermal treatment.

In any test, a specimen was stretched with a cross-head speed of 10 mm/min (which corresponds to the Hencky strain rate $\dot{\epsilon}_H = 2.09 \cdot 10^{-4}\ \mathrm{s}^{-1}$) up to the maximal strain, ϵ_{max}, and unloaded with the same cross-head speed to the zero stress. The chosen cross-head speed ensures nearly isothermal experimental conditions [27], on the one hand, and it is sufficiently large to disregard the viscoelastic effects, on the other (the maximal duration of a loading test does not exceed 1 min).

Any series of experiments consisted of 6 tests with the maximal strains $\epsilon_{max} = 0.02$, 0.04, 0.06, 0.08, 0.10 and 0.12. Each test was performed on a new specimen. The interval of strains under consideration includes the entire sub-yield region (the yield strain for a non-annealed iPP $\epsilon_y = 0.13$, according to the supplier). We confine ourselves to relatively small deformations, because the purpose of the study is to approximate experimental data by using constitutive equations with small strains.

For the sake of brevity, we present only the stress–strain curves for specimens annealed at 140 °C. The engineering stresses, σ, is plotted versus the engineering strain, ϵ, in Figures 1 to 6. The stress–strain diagrams for non-annealed specimens, as well as for

samples annealed at 120 and 160 °C have a similar shape. The following features of the experimental curves are worth to be mentioned:

1. at all maximal strains, $\epsilon_{\max}$, the stress–strain curves corresponding to the loading and unloading paths substantially differ from each other,

2. the unloading curves are strongly nonlinear,

3. the residual strain (measured at the instant when the stress vanishes) noticeably increases with the maximal strain, $\epsilon_{\max}$.

3 A micro-mechanical model

A semicrystalline polymer is treated as an equivalent network of chains. The network is assumed to be strongly heterogeneous. This heterogeneity is attributed to an inhomogeneity of interactions between chains in the amorphous phase and crystalline lamellae with various lengths and thicknesses. The network is modelled as an ensemble of meso-regions (MRs) with arbitrary shapes. The characteristic length of a MR substantially exceeds the radius of gyration for a macromolecule, and it is noticeably less than a size of a sample.

Deformation of a specimen induces two processes in the network:

1. Sliding of junctions (physical cross-links and entanglements that bridge chains in the network) with respect to their positions in the stress-free state.

2. Sliding of meso-domains in the ensemble with respect to each other.

Sliding of junctions describes non-affine deformation of the network. This process is determined by a plastic strain $\epsilon_{\rm p1}$. Sliding of MRs with respect to each other is described by a plastic strain $\epsilon_{\rm p2}$. In a semicrystalline polymer, the strain $\epsilon_{\rm p1}$ reflects sliding of junctions in the amorphous phase, slippage of tie chains and fine slip of lamellar blocks. The strain $\epsilon_{\rm p2}$ characterizes coarse slip of lamellar blocks and their disintegration.

The total plastic strain, $\epsilon_{\rm p}$, equals the sum of the plastic strains driven by sliding of nodes and mutual displacements of meso-domains,

$$\epsilon_{\rm p} = \epsilon_{\rm p1} + \epsilon_{\rm p2}. \tag{1}$$

We suppose that meso-domains are connected by links that transmit the macro-strain, ϵ, to individual MRs. This implies the conventional hypothesis that the macro-strain, ϵ, equals the sum of the elastic strain in meso-regions, $\epsilon_{\rm e}$, and the plastic strain, $\epsilon_{\rm p}$,

$$\epsilon = \epsilon_{\rm e} + \epsilon_{\rm p}. \tag{2}$$

To simplify the analysis, we assume that the elastic strains in various MRs coincide.

Deformation of a specimen results in evolution of the plastic strain, $\epsilon_{\rm p1}$, both at the stages of active loading and unloading. We suppose that the rate of changes in the plastic strain, $\epsilon_{\rm p1}$, is proportional to the rate of changes in the macro-strain, ϵ,

$$\frac{d\epsilon_{\rm p1}}{dt}(t) = \varphi(\epsilon_{\rm e}(t))\frac{d\epsilon}{dt}(t), \tag{3}$$

where the coefficient of proportionality, φ, depends on the elastic strain $\epsilon_{\rm e}$. It is assumed that the function $\varphi(\epsilon_{\rm e})$ vanishes at the zero elastic strain, $\varphi(0) = 0$, monotonically increases with $\epsilon_{\rm e}$, and tends to some constant $a \in [0, 1]$ for relatively large elastic strains,

$$\lim_{\epsilon_{\rm e}\to\infty} \varphi(\epsilon_{\rm e}) = a,$$

where a is the rate of sliding of junctions in MRs corresponding to a developed plastic flow. The inequality $a \geq 0$ means that junctions slide in the direction that is determined by the macro-strain ϵ. The condition $a \leq 1$ ensures that the rate of sliding does not exceed the rate of straining.

To approximate experimental data, we employ the function

$$\varphi(\epsilon_{\rm e}) = a\Big[1 - \exp\Big(-\frac{\epsilon_{\rm e}}{\varepsilon}\Big)\Big]. \tag{4}$$

This function is determined by two adjustable parameters, a and ε, where the quantity ε characterizes how "large" an elastic strain, $\epsilon_{\rm e}$, is.

With reference to [1, 5], we suppose that under active loading in the sub-yield region, lamellar fragmentation does not occur and the plastic strain $\epsilon_{\rm p2}$ vanishes,

$$\frac{d\epsilon_{\rm p2}}{dt}(t) = 0 \qquad \Big(\frac{d\epsilon}{dt}(t) \geq 0, \quad \sigma(t) \geq 0\Big). \tag{5}$$

According to Eq. (5), the entire dissipation of energy at active deformation is attributed to sliding of junctions with respect to their reference positions, whereas displacements of MRs with respect to each other are disregarded.

It is assumed that under unloading, meso-domains slide with respect to each other as they are driven by a positive macro-stress σ. These mutual displacements of MRs are characterized by a plastic strain, $\epsilon_{\rm p2}$, that grows with time t. An increase in $\epsilon_{\rm p2}$ during unloading reflects coarse slip and fragmentation of deformed lamellae. The evolution of the plastic strain, $\epsilon_{\rm p2}$, is described by the flow rule

$$\frac{d\epsilon_{\rm p2}}{dt}(t) = -K\sigma(t)\frac{d\epsilon}{dt}(t) \qquad \Big(\frac{d\epsilon}{dt}(t) < 0, \quad \sigma(t) \geq 0\Big). \tag{6}$$

Equation (6) means that the rate of changes in $\epsilon_{\rm p2}$ is proportional to the rate of work of external loads

$$J(t) = -\sigma(t)\frac{d\epsilon}{dt}(t),$$

where the sign "$-$" accounts for the opposite directions of the longitudinal stress and the strain increment. With reference to [28], we suppose that the coefficient of proportionality, $K \geq 0$, is a function of the maximal plastic strain, $\epsilon_{\rm p1}$, reached: $K = K(\epsilon^{\circ}_{\rm p1})$, where

$$\epsilon^{\circ}_{\rm p1}(t) = \max_{0\leq\tau\leq t} \epsilon_{\rm p1}(\tau).$$

To match observations, we use the linear function

$$K = K_0 + K_1\epsilon^{\circ}_{\rm p1}, \tag{7}$$

where K_m $(m = 0, 1)$ are adjustable parameters. Equation (7) means that the larger is the plastic strain, $\epsilon_{\rm p1}$, driven by fine slip of lamellar blocks under active loading, the higher is the rate of the plastic strain, $\epsilon_{\rm p2}$, that reflects coarse slip and fragmentation of lamellae at unloading.

Separation of tie chains from lamellae and disintegration of lamellar blocks result in a decrease in the number of MRs to which the macro-strain, ϵ, is transmitted by surrounding meso-domains. This decrease is attributed to two different processes: (i) mechanically-induced separation of individual MRs from the ensemble, and (ii) screening of meso-domains by stacks of disintegrated lamellae.

To describe evolution of an ensemble of meso-domains, we introduce the average number of MRs, N_0, per unit mass of a virgin specimen (where all MRs are connected with one another) and the average number of MRs, $N(t)$, in the deformed specimen at time $t \geq 0$ (where some meso-regions are separated from the ensemble).

At the stage of active loading in the sub-yield region, separation of MRs from the ensemble does not take place, which implies that $N(t)$ remains constant,

$$\frac{dN}{dt}(t) = 0 \qquad \Big(\frac{d\epsilon}{dt}(t) \geq 0, \quad \sigma(t) \geq 0\Big), \qquad N(0) = N_0. \tag{8}$$

Changes in the function $N(t)$ at unloading are governed by a first order kinetic equation, according to which the relative number of MRs separated from the ensemble per unit time is proportional to the increment of the plastic strain, $\epsilon_{\rm p2}$,

$$-\frac{1}{N(t)}\frac{dN}{dt}(t) = \kappa\frac{d\epsilon_{\rm p2}}{dt}(t) \qquad \Big(\frac{d\epsilon}{dt}(t) < 0, \quad \sigma(t) \geq 0\Big). \tag{9}$$

By analogy with Eq. (6), the coefficient $\kappa > 0$ is treated as a function of the maximal plastic strain $\epsilon^{\circ}_{\rm p1}$: $\kappa = \kappa(\epsilon^{\circ}_{\rm p1})$. The pre-factor κ in Eq. (9) is assumed to be rather large for small plastic strains, $\epsilon_{\rm p1}$, i.e., when straining of a specimen produces no fine slip of lamellar blocks, and it monotonically decreases with $\epsilon_{\rm p1}$. This decrease is attributed to alignment of lamellar blocks driven by their fine slip, which, in turn, diminishes the probability of formation of disordered lamellar stacks at unloading. These stacks do not transmit the macro-strain, ϵ, to the amorphous domains surrounded by them, which results in isolation of these regions from the ensemble (in a way silimar to the formation of regions of occluded rubber in particle-reinforced elastomers [29]).

To fit experimental data, we adopt the function

$$\kappa = \kappa_0 + \kappa_1 \exp\Big(-\frac{\epsilon^{\circ}_{\rm p1}}{e_*}\Big), \tag{10}$$

where κ_m $(m = 0, 1)$ and e_* are adjustable parameters. Equation (10) implies that κ monotonically decreases from the initial value $\kappa_0 + \kappa_1$ and tends to the limiting value κ_0 at relatively large plastic strains, $\epsilon_{\rm p1}$. The quantity e_* indicates how "large" the maximal plastic strain, $\epsilon^{\circ}_{\rm p1}$, is.

4 Constitutive equations

Under isothermal uniaxial deformation, a meso-domain is treated as a linear elastic solid with the mechanical energy

$$w = \frac{1}{2}\mu\epsilon_{\rm e}^2,$$

where the constant $\mu > 0$ is the average rigidity of a MR. Neglecting the energy of interaction between meso-regions, we calculate the strain energy density per unit mass of a polymer as the sum of the mechanical energies of MRs,

$$W(t) = \frac{\mu}{2}N(t)\epsilon_{\rm e}^2. \tag{11}$$

It follows from Eqs. (1) to (3) and (11) that the derivative of the function W with respect to time is given by

$$\frac{dW}{dt}(t) = \frac{\mu}{2}\frac{dN}{dt}(t)\epsilon_{\rm e}^2(t) + \mu N(t)\epsilon_{\rm e}(t)\Big[\Big(1-\varphi(\epsilon_{\rm e}(t))\Big)\frac{d\epsilon}{dt}(t) - \frac{d\epsilon_{\rm p2}}{dt}(t)\Big]. \tag{12}$$

The Clausius-Duhem inequality reads

$$Q(t) = -\frac{dW}{dt}(t) + \frac{1}{\rho}\sigma(t)\frac{d\epsilon}{dt}(t) \geq 0,$$

where ρ is mass density, and Q is internal dissipation per unit mass. Substition of Eq. (12) into this formula results in

$$Q(t) = \frac{1}{\rho}\Big[\sigma(t) - \rho\mu N(t)\epsilon_{\rm e}(t)\Big(1-\varphi(\epsilon_{\rm e}(t))\Big)\Big]\frac{d\epsilon}{dt}(t) + Y(t) \geq 0, \tag{13}$$

where

$$Y(t) = \mu N(t)\epsilon_{\rm e}(t)\Big[\frac{d\epsilon_{\rm p2}}{dt}(t) - \frac{1}{2N(t)}\frac{dN}{dt}(t)\epsilon_{\rm e}(t)\Big]. \tag{14}$$

Equating the expression in square brackets in Eq. (13) to zero, we find that

$$\sigma(t) = E(t)\epsilon_{\rm e}(t)\Big[1-\varphi(\epsilon_{\rm e}(t))\Big] \tag{15}$$

with

$$E(t) = \rho\mu N(t). \tag{16}$$

Equations (5), (8) and (14) imply that the function Y vanishes at active loading,

$$Y(t) = 0 \qquad \Big(\frac{d\epsilon}{dt}(t) \geq 0, \quad \sigma(t) \geq 0\Big). \tag{17}$$

It follows from Eqs. (6), (9), and (14) to (16) that at unloading,

$$Y(t) = -\frac{K}{\rho}\Big(1+\frac{\kappa}{2}\Big)\frac{\sigma^2(t)}{1-\varphi(\epsilon_{\rm e}(t))}\frac{d\epsilon}{dt}(t) \qquad \Big(\frac{d\epsilon}{dt}(t) < 0, \quad \sigma(t) \geq 0\Big). \tag{18}$$

Combining Eqs. (13), (15) and (16), we find that the internal dissipation per unit mass, $Q(t)$, coincides with $Y(t)$. According to Eqs. (17) and (18), the function $Y(t)$ is non-negative. This means that the Clausius–Duhem inequality is satisfied for an arbitrary deformation program, provided that the stress, σ, is given by Eq. (15).

It follows from Eqs. (8), (9) and (16) that the elastic modulus, E, obeys the differential equations

$$\begin{aligned} &\frac{dE}{dt}(t) = 0, \quad E(0) = E_0 \qquad \Big(\frac{d\epsilon}{dt}(t) \geq 0, \quad \sigma(t) \geq 0\Big), \\ &\frac{1}{E(t)}\frac{dE}{dt}(t) = -\kappa\frac{d\epsilon_{\rm p2}}{dt}(t) \qquad \Big(\frac{d\epsilon}{dt}(t) < 0, \quad \sigma(t) \geq 0\Big), \end{aligned} \tag{19}$$

where $E_0 = \mu\rho N_0$ is the elastic modulus for a virgin specimen.

The assumption that elastic moduli are strongly affected by mechanical factors is widely used in elastoplasticity theories for geomaterials [30, 31]. For granular media, this effect is attributed to the growth of voids between particles under active loading and to the contractive response at unloading (which means that elastic moduli become functions of the volumetric strain [31]). In the present model, the plastic strain, $\epsilon_{\rm p2}$, plays a role similar to that the mean elastic strain plays in elastoplasticity theories for granular materials: it characterizes the level of disorder produced by mechanically-induced lamellar fragmentation. The difference between our approach and previous studies is that for an arbitrary time-dependent loading program, the elastic modulus, E, depends not on the current strain, but on the entire history of deformation [because Eqs. (19) cannot be integrated explicitly when κ is a function of the maximal plastic strain, $\epsilon^{\circ}_{\rm p1}$, reached under active loading].

Uniaxial deformation of a semi-crystalline polymer is described by Eqs. (1), (2), (4) to (6), (15) and (19). Any stress–strain curve for cyclic loading is determined by 5 adjustable parameters:

1. the initial elastic modulus E_0,
2. the rate of a developed plastic flow a,
3. the strain ε that characterizes transition to a steady plastic flow,
4. the rate of sliding of MRs with respect to each other $K = K(\epsilon^{\circ}_{\rm p1})$,
5. the rate of separation of meso-domains from an ensemble $\kappa = \kappa(\epsilon^{\circ}_{\rm p1})$.

This number is quite comparable with the number of material constants in other constitutive models in elastoplasticity, see, e.g., [22, 23, 25]. It should be noted, however, that most of these concepts fail to adequately describe the mechanical behavior of polymers in cyclic tests [32].

An important advantage of the stress–strain relations (1), (2), (4) to (6), (15) and (19) is that 3 constants, E_0, a and ε, are found by fitting experimental data for the loading path of a stress–strain curve, whereas the other two parameters, K and κ, are determined by matching observations for the unloading path.

The dependences of K and κ on the maximal plastic strain, $\epsilon^{\circ}_{\rm p1}$, are described by Eqs. (7) and (10). To find the coefficients K_m, κ_m and e_* is these equations, the quantities K and κ (determined by matching observations in a series of cyclic tests with various maximal strains $\epsilon_{\max}$) are approximated by functions (7) and (10).

5 Fitting of observations

We begin with the approximation of the stress–strain diagrams for active loading. It follows from Eqs. (1), (2), (4), (5), (15) and (19) that the stress, σ, is given by

$$\sigma(\epsilon) = E_0(\epsilon - \epsilon_{\rm p1})\Big\{1 - a\Big[1 - \exp\Big(-\frac{\epsilon - \epsilon_{\rm p1}}{\varepsilon}\Big)\Big]\Big\}, \tag{20}$$

where the plastic strain, $\epsilon_{\rm p1}$, satisfies the nonlinear differential equation

$$\frac{d\epsilon_{\rm p1}}{d\epsilon}(\epsilon) = a\Big[1 - \exp\Big(-\frac{\epsilon - \epsilon_{\rm p1}}{\varepsilon}\Big)\Big], \qquad \epsilon_{\rm p1}(0) = 0. \tag{21}$$

The loading path of any stress–strain curve is determined by 3 material constants: E_0, a and ε. To find these quantities, we fix some intervals $[0, a_{\max}]$ and $[0, \varepsilon_{\max}]$, where the "best-fit" parameters a and ε are assumed to be located, and divide these intervals into J subintervals by the points $a_i = i\Delta a$ and $\varepsilon_j = j\Delta\varepsilon$ $(i, j = 1, \ldots, J)$ with $\Delta a = a_{\max}/J$ and $\Delta\varepsilon = \varepsilon_{\max}/J$. For any pair, $\{a_i, \varepsilon_j\}$, Eq. (21) is integrated numerically by the Runge–Kutta method with the step $\Delta\epsilon = 1.0 \cdot 10^{-5}$. Given a pair, $\{a_i, \epsilon_j\}$, the elastic modulus, $E_0 = E_0(i, j)$, is found by the least-squares method from the condition of minimum of the function

$$F(i, j) = \sum_{\epsilon_m} \Big[\sigma_{\rm exp}(\epsilon_m) - \sigma_{\rm num}(\epsilon_m)\Big]^2,$$

where the sum is calculated over all experimental points, ϵ_m, on a loading path, $\sigma_{\rm exp}$ is the stress measured in a tensile test, and $\sigma_{\rm num}$ is given by Eq. (20). The "best-fit" parameters a and ε are determined from the condition of minimum of the function F on the set $\{a_i, \varepsilon_j \quad (i, j = 1, \ldots, J)\}$.

The material constants E_0, a and ε that minimize the discrepancies between the experimental data and the results of numerical analysis are found for any stress–strain curve independently. Afterwards, we calculate the average values of these quantities and their standard deviations for 4 series of tests. These values are presented in Table 1 for non-annealed specimens and for samples annealed at 120, 140 and 160 °C. The table shows that the elastic modulus, E_0, and the rate of developed plastic flow, a, are determined with a high level of accuracy (the relative deviations are less than 8 and 13 %, respectively), whereas the accuracy in determining the strain, ε, that characterizes transition to a steady-state plastic flow, is rather low (about 29 %).

To find the quantities K and κ, we approximate the unloading paths of the stress–strain curves. It follows from Eqs. (1), (2), (4), (6), (15) and (18) that the stress, σ, is given by

$$\sigma(\epsilon) = E(\epsilon_{\rm p2})(\epsilon - \epsilon_{\rm p1} - \epsilon_{\rm p2})\Big\{1 - a\Big[1 - \exp\Big(-\frac{\epsilon - \epsilon_{\rm p1} - \epsilon_{\rm p2}}{\varepsilon}\Big)\Big]\Big\}, \tag{22}$$

where the elastic modulus, E, reads

$$E(\epsilon_{\rm p2}) = E_0 \exp(-\kappa\epsilon_{\rm p2}). \tag{23}$$

The plastic strains, $\epsilon_{\rm p1}$ and $\epsilon_{\rm p2}$, obey the differential equations

$$\frac{d\epsilon_{\rm p1}}{d\epsilon}(\epsilon) = a\Big[1 - \exp\Big(-\frac{\epsilon - \epsilon_{\rm p1} - \epsilon_{\rm p2}}{\varepsilon}\Big)\Big], \qquad \frac{d\epsilon_{\rm p2}}{d\epsilon}(\epsilon) = -K\sigma(\epsilon) \tag{24}$$

with the "initial" conditions

$$\epsilon_{\rm p1}(\epsilon_{\max}) = \epsilon^{\circ}_{\rm p1}, \qquad \epsilon_{\rm p2}(\epsilon_{\max}) = 0.$$

To approximate experimental data in a cyclic test with a maximal tensile strain $\epsilon_{\max}$, we apply an algorithm similar to that used to match the stress–strain curves at active loading. We fix some intervals $[0, K_{\max}]$ and $[0, \kappa_{\max}]$, where the "best-fit" parameters K and κ are assumed to be located, and divide these intervals into J subintervals by the points $K_i = i\Delta K$ and $\kappa_j = j\Delta\kappa$ $(i, j = 1, \ldots, J)$ with $\Delta K = K_{\max}/J$ and $\Delta\kappa = \kappa_{\max}/J$. For any pair, $\{K_i, \kappa_j\}$, Eqs. (20) to (22) are integrated numerically by the Runge–Kutta method with the step $\Delta\epsilon = 1.0 \cdot 10^{-5}$ and with the value of E_0 found by fitting the loading paths of the stress–strain curves. The "best-fit" parameters K and κ are determined from the condition of minimum of the function F on the set $\{K_i, \kappa_j \quad (i, j = 1, \ldots, J)\}$.

The parameter K is plotted versus $\epsilon^{\circ}_{\rm p1}$ in Figure 7. The maximal plastic strain, $\epsilon^{\circ}_{\rm p1}$, is determined by numerical integration of Eq. (21) from $\epsilon = 0$ to $\epsilon = \epsilon_{\max}$. The experimental data are fitted by Eq. (7), where the coefficients K_m $(m = 0, 1)$ are found by the least-squares technique.

The quantity κ is depicted as a function of $\epsilon^{\circ}_{\rm p1}$ in Figure 8 together with its approximation by Eq. (10). The strain e_* is determined by the steepest-descent method, whereas the coefficients κ_m $(m = 0, 1)$ are calculated by the least-squares algorithm. Unlike Figure 7, where the only curve provides an acceptable approximation of all experimental data, adjustable parameters in Eq. (10) are found independently for specimens not-subjected to thermal treatment and annealed at temperatures in the low-temperature region, on the one hand, and for samples annealed at 160 °C, on the other.

6 Discussion

Figure 1 to 6 demonstrate fair agreement between the observations in loading–unloading tests with various maximal strains, $\epsilon_{\max}$, and the results of numerical simulation. The same quality of fitting has been reached also for the stress–strain curves for specimens not subjected to thermal treatment and those annealed at 120 and 140 °C. These figures confirm that the model correctly describes the mechanical response of semicrystalline polymers in cyclic tests.

Table 1 shows that annealing of iPP in the low-temperature region does not affect the elastic modulus, E_0, and the rate of developed plastic flow, a. Annealing at 160 °C causes a noticeable increase (from 20 to 30 %) in the elastic modulus, E_0, and a growth of the rate of steady plastic flow, a, that reaches its ultimate value. Although the increase in

a is not rather high (about 6 to 14 %), the fact that the rate of developed plastic flow reaches unity means that at relatively large elongations, the elastic strain, $\epsilon_{\rm e}$, does not grow, and an increase in the macro-strain, ϵ, is totally compensated by the same increase in the plastic strain, $\epsilon_{\rm p1}$. On the contrary, the rate of developed plastic flow in specimens not subjected to thermal treatment, as well as in those annealed in the low-temperature region is noticeably less than unity, which implies a strong increase in the elastic strain under stretching. This difference becomes important for the analysis of stress–strain curves at large elongations (appropriate data are not presented): necking of specimens not subjected to annealing occurs at the Hencky strains about 0.2, whereas necking of specimens annealed in the high-temperature region is not observed at the Hencky strains up to 0.6 .

The growth of the elastic modulus, E_0, of specimens annealed at 160 °C may be attributed to an increase in perfectness of crystalline lamellae (associated with transition from a statistically disordered α_1 phase into an ordered α_2 phase characterized by regularity in the up and down positions of methyl groups along the chains [19]). An increase in the rate of developed plastic flow, a, may be ascribed to a decrease in the level of cross-hatching in α spherulites with the growth of annealing temperature [16] and the total disappearance of transverse lamellae above the critical temperature $T_{\rm c}$ = 159 °C [19].

Table 1 shows that the parameter ε is independent of the annealing temperature (within the range of experimental uncertainities). This conclusion appears to be quite natural, because ε characterizes sliding of junctions between chains in MRs. This quantity describes the response of the amorphous phase that is not affected by thermal treatment. The value of ε (in the range between 3 and 4 %) found by fitting the stress–strain curves appears to be rather close to a critical strain, $\epsilon_{\rm c}$, determined by matching relaxation curves [33] as the strain at which the rate of relaxation becomes independent of mechanical factors.

Figure 7 reveals that the parameter K is not affected by annealing temperature. At first glance, this result seems rather surprising, because K is responsible for mutual displacements of MRs driven by coarse slip and fragmentation of lamellar blocks. Two explanations may be provided for our findings. The first is based on the Nitta–Takayanagi [4] and Meyer–Pruitt [34] concepts that attribute plastic deformation of semicrystalline polymers to slippage of tie chains along lamellae and pulling out of chains from disintegrated lamellar blocks (both processes are associated with transformations in the amorphous phase whose state is not influenced by thermal treatment). The other explanation is based on the assumption that an increase in perfectness of crystallites at annealing (which makes lamellae stronger) is compensated by disappearance of tangential lamellae (which results in weakening of spherulites). Because these morphological transformations in iPP lead to opposite changes in the mechanical response, their combined effect may be negligible.

According to Figure 8, the parameter κ is not affected by annealing in the low-temperature region, but is strongly influenced by high-temperature annealing. The limiting value of this quantity, κ_0, that corresponds to a developed plastic flow at unloading, increases approximately by twice after annealing at 160 °C. Because κ characterizes changes in the elastic modulus driven by lamellar fragmentation, see Eq. (19), we associate this

growth with weakening of spherulites induced by disappearance of cross-hatching.

The strain, e_*, that determines transition to a steady plastic flow at unloading (for all specimens, but those annealed at 160 °C) is very close to the strain, ε, that characterizes transition to a developed plastic flow at active loading. This implies an opportunity to reduce the number of adjustable parameters in the constitutive equations by replacing e_* by ε. However, an additional analysis of the physical basis for this simplification is required.

7 Concluding remarks

Four series of tensile loading–unloading tests have been performed on injection-molded isotactic polypropylene at room temperature. In the first series, specimens were used as produced, whereas in the other series, samples were annealed for 24 h at 120, 140 and 160 °C prior to testing.

Constitutive equations have been derived for the elastoplastic response of semicrystalline polymers. A polymer is treated as an equivalent network of chains bridged by junctions. The network is assumed to be strongly heterogeneous, and it is modelled as an ensemble of meso-regions linked with each other. Under active loading in the sub-yield region of deformations, junctions between chains in MRs slide with respect to their reference positions (which describes sliding of tie chains and fine slip of lamellar blocks). At unloading, this non-affine deformation of the network is accompanied by displacements of meso-domains with respect to each other (which describes coarse slip and fragmentation of lamellar blocks). Destructure of lamellae results in separation of some MRs from the ensemble (driven by breakage of links between isolated meso-domains and the network and screening of macro-strain in these meso-domains by surrounding stacks of disintegrated lamellae.

Kinetic equations are proposed for the rates of two plastic strains that describe these processes and for the rate of separation of MRs from an ensemble. Stress–strain relations for isothermal uniaxial deformation are developed by using the laws of thermodynamics. The constitutive equations are determined by 5 adjustable parameters that are found by fitting the experimental data. Fair agreement is demonstrated between the experimental stress–strain curves and the results of numerical simulation.

The following conclusions are drawn:

1. Annealing in the low-temperature region does not affect the material constants that reflect the elastoplastic response of iPP.

2. Annealing in the high-temperature region results in an increase in the elastic modulus E_0 (which is attributed to the growth of the perfectness of crystals induced by $\alpha_1 \to \alpha_2$ transition).

3. Annealing in the high-temperature region causes the growth of the rate of developed plastic flow a (that reaches its ultimate value) and an increase in the rate of separation of meso-regions from an ensemble κ (these changes are associated with disappearance of transversal lamellae).

4. The rate of plastic strain, K, linearly grows with the maximal plastic strain, $\epsilon^{\circ}_{\mathrm{p1}}$, which means that sliding of junctions in MRs under active loading activates coarse slip and fragmentation of lamellae at unloading. The activation process appears to be independent of the perfectness of crystallites.

5. The strains ε and e_* that characterize transitions to steady plastic flows at active loading and unloading, respectively, are rather close to each other and are weakly affected by thermal treatment. This result confirms the hypothesis [4, 34] that elastoplastic deformation of a semicrystalline polymer in a sub-yield region is mainly associated with transformations in the amorphous phase.

References

[1] Aboulfaraj M, G'Sell C, Ulrich B, Dahoun A. Polymer 1995;36:731.

[2] Uzomah TC, Ugbolue SCO. J Appl Polym Sci 1997;65:625.

[3] Coulon G, Castelein G, G'Sell C. Polymer 1998;40:95.

[4] Nitta K-H, Takayanagi M. J Polym Sci Part B: Polym Phys 1999;37:357.

[5] Seguela R, Staniek E, Escaig B, Fillon B. J Appl Polym Sci 1999;71:1873.

[6] Staniek E, Seguela R, Escaig B, Francois P. J Appl Polym Sci 1999;72:1241.

[7] Nitta K-H, Takayanagi M. J Polym Sci Part B: Polym Phys 2000;38:1037.

[8] Labour T, Gauthier C, Seguela R, Vigier G, Bomal Y, Orange G. Polymer 2001;42:7127.

[9] Lima MFS, Vasconcellos MAZ, Samios D. J Polym Sci Part B: Polym Phys 2002;40:896.

[10] Iijima M, Strobl G. Macromolecules 2000;33:5204.

[11] Kalay G, Bevis MJ. J Polym Sci Part B: Polym Phys 1997;35:241,265.

[12] Maiti P, Hikosaka M, Yamada K, Toda A, Gu F. Macromolecules 2000;33:9069.

[13] Verma R, Marand H, Hsiao B. Macromolecules 1996;29:7767.

[14] Zhang XC, Butler MF, Cameron RE. Polym Int 1999;48:1173.

[15] Al-Raheil IA, Qudah AM, Al-Share M. J Appl Polym Sci 1998;67:1267.

[16] Yamada K, Matsumoto S, Tagashira K, Hikosaka M. Polymer 1998;39:5327.

[17] Xu J, Srinivas S, Marand H, Agarwal P. Macromolecules 1998;31:8230.

[18] Alamo RG, Brown GM, Mandelkern L, Lehtinen A, Paukkeri R. Polymer 1999;40: 3933.

[19] Gu F, Hikosaka M, Toda A, Ghosh SK, Yamazaki S, Araki M, Yamada K. Polymer 2002;43:1473.

[20] Drozdov AD, Christiansen JdeC. Polymer 2002;accepted.

[21] Boyce MC, Parks DM, Argon AS. Mech Mater 1988;7:15.

[22] Hasan OA, Boyce MC. Polym Eng Sci 1995;35:331.

[23] Bordonaro CM, Krempl E. Polym Eng Sci 1995;35:310.

[24] Quinson R, Perez J, Rink M, Pavan A. J Mater Sci 1997;32:1371.

[25] Spathis G, Kontou E. Polymer 1998;39:135.

[26] Ogden RW, Roxburgh DG. Proc Roy Soc London A 1999;455:2861.

[27] Inberg JPF, Takens A, Gaymans RJ. Polymer 2002;43:2795.

[28] Miehe C. Eur J Mech A/Solids 1995;14:697.

[29] Witten TA, Rubinstein M, Colby RH. J Phys II (France) 1993;3:367.

[30] Houlsby GT. Comput Geotech 1985;1:3.

[31] Rouainia M, Muir Wood D. Mech Cohes-Frict Mater 2000;5:469.

[32] Bergstrom JS, Kurtz SM, Rimnac CM, Edidin AA. Biomaterials 2002;23:2329.

[33] Drozdov AD, Christiansen JdeC. J Appl Polym Sci 2002;accepted.

[34] Meyer RW, Pruitt LA. Polymer 2001;42:5293.

List of figures

Table 1: Adjustable parameters E_0 GPa, a and ε for specimens annealed at various temperatures T °C (the values in parentheses indicate standard deviations)

T	E_0	a	$\varepsilon \cdot 10^2$
non-annealed	1.81 (0.11)	0.93 (0.04)	3.84 (0.53)
120	1.75 (0.08)	0.87 (0.09)	3.52 (0.50)
140	1.71 (0.14)	0.91 (0.12)	4.18 (1.23)
160	2.18 (0.12)	0.99 (0.01)	3.84 (0.33)

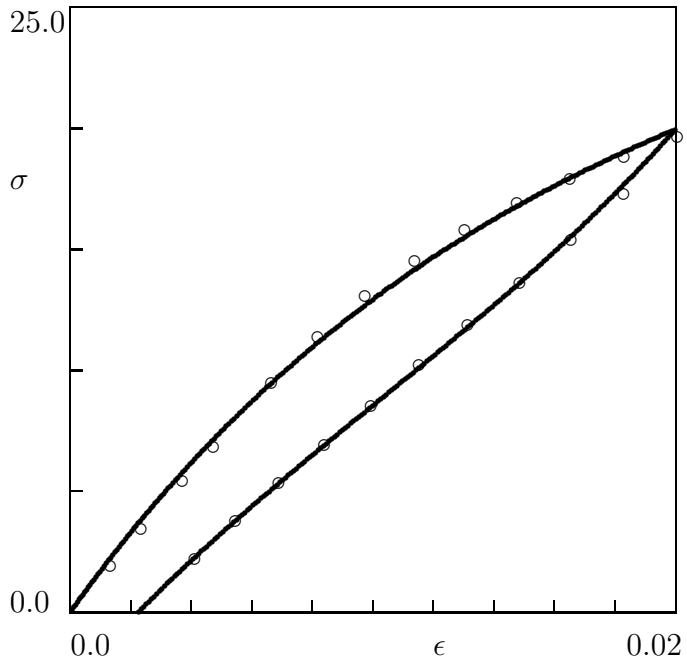

Figure 1:

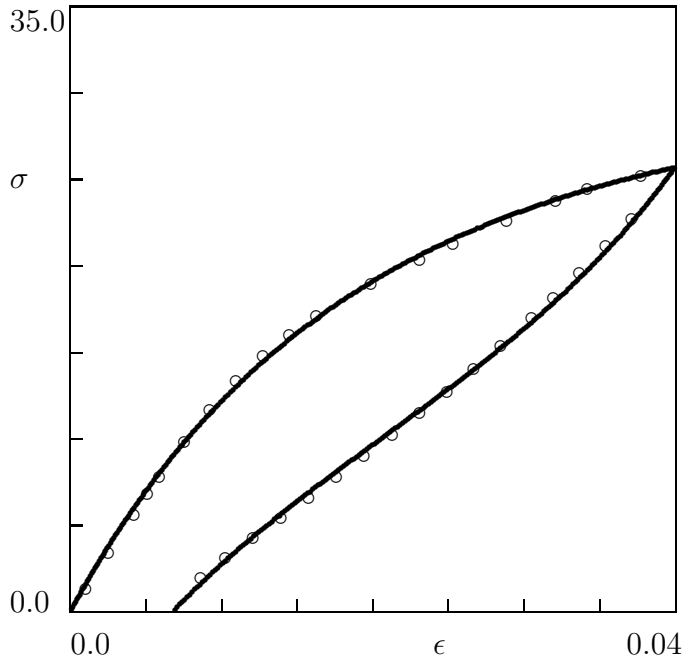

Figure 2:

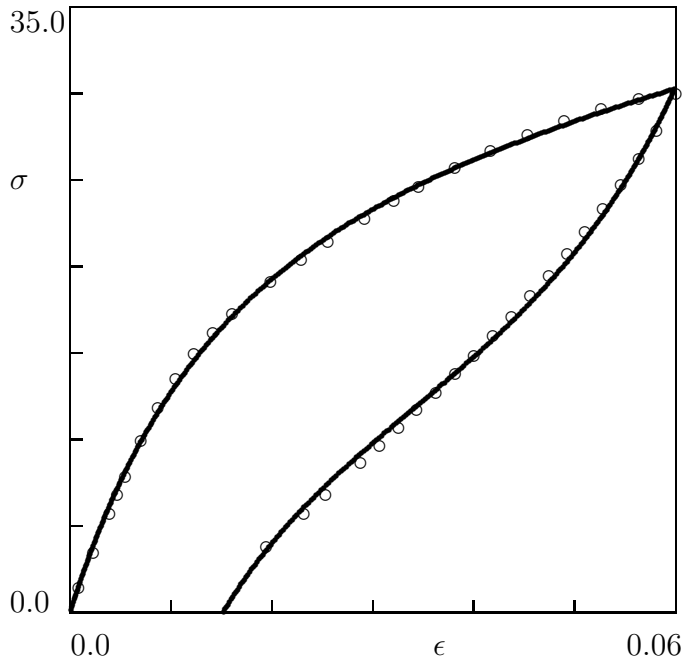

Figure 3:

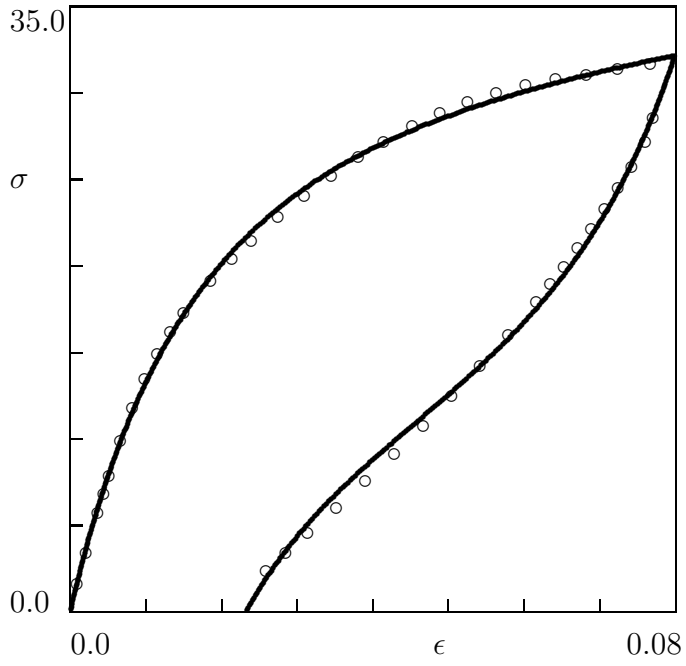

Figure 4:

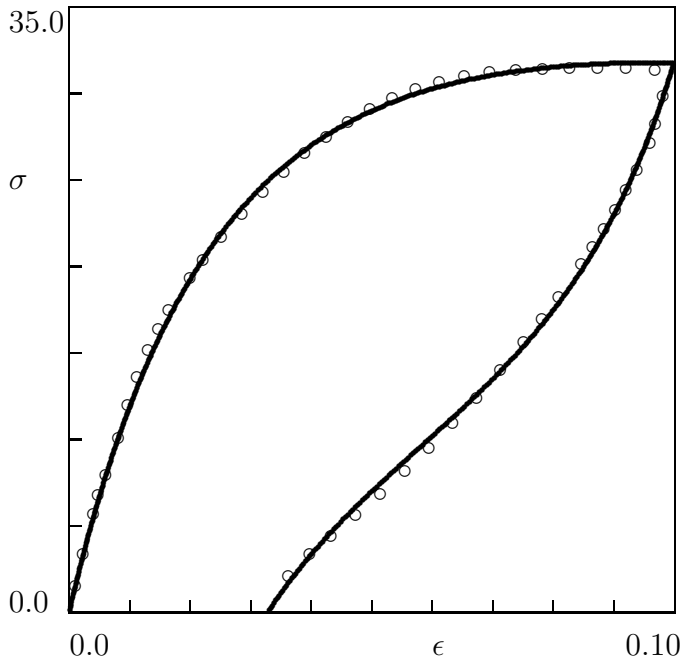

Figure 5:

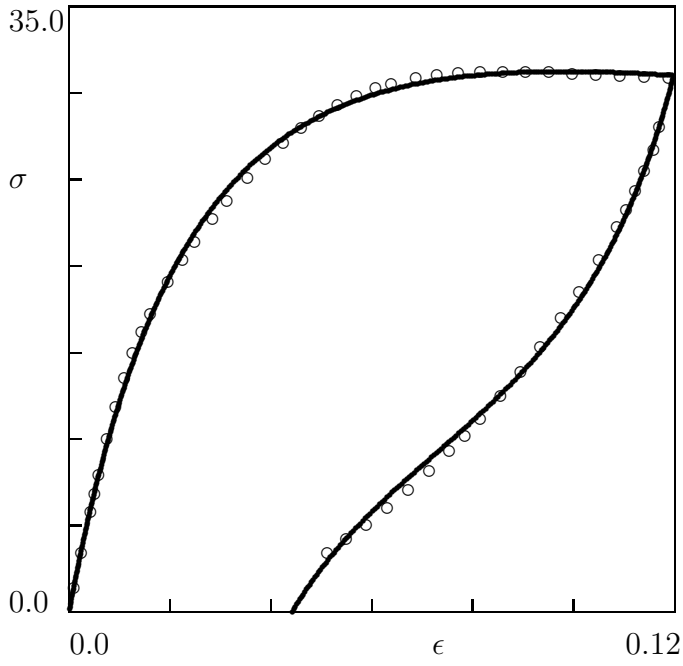

Figure 6:

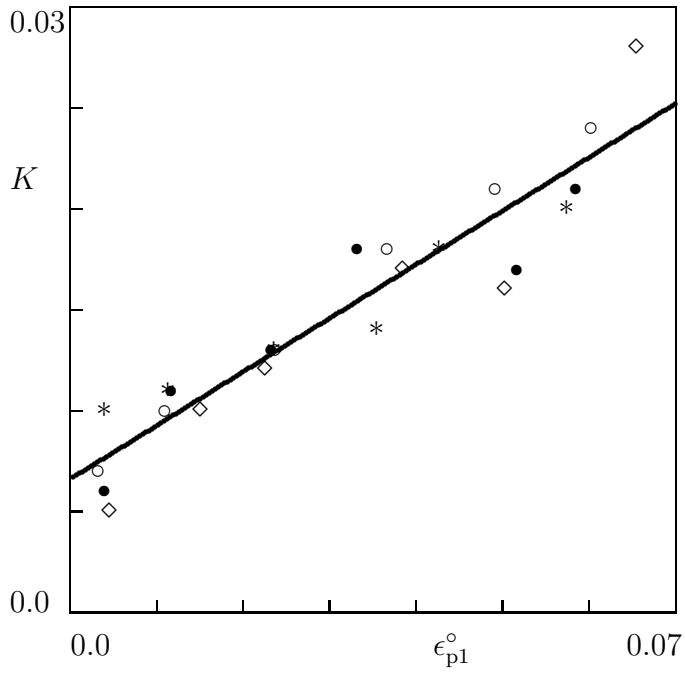

Figure 7:

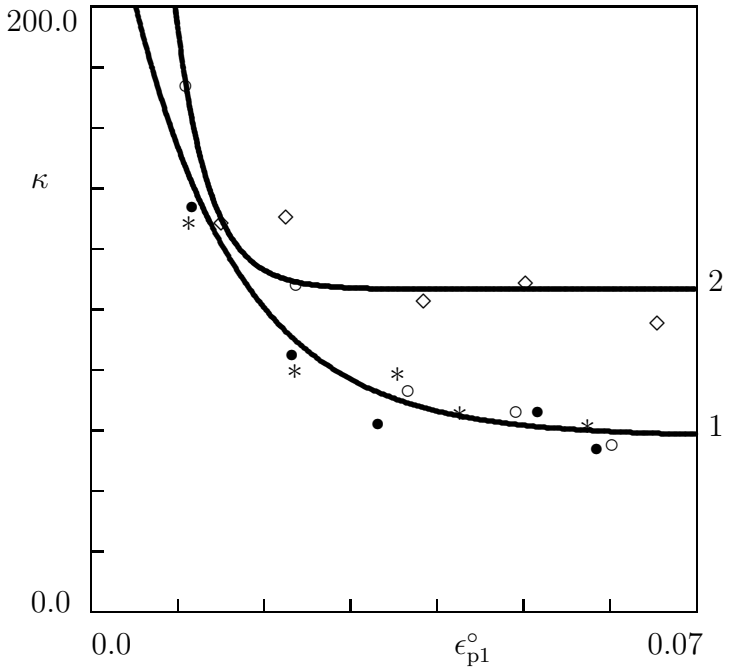

Figure 8: